Scanning Inverse Fluorescence Correlation Spectroscopy

Jan Bergstrand[a], Daniel Rönnlund[a], Jerker Widengren[a], Stefan Wennmalm[b*]

[a] Experimental Biomolecular Physics, Royal Institute of Technology-KTH, Albanova University Center, 106 91 Stockholm, Sweden
[b] Experimental Biomolecular Physics, Royal Institute of Technology-KTH, SciLifeLab, 171 65 Solna, Sweden

ABSTRACT

Inverse Fluorescence Correlation Spectroscopy (iFCS) analyses unlabeled particles by detecting signals from molecules surrounding the particles of interest. As the particles traverse the fL detection volume they displace a fraction of the signal-generating molecules, and create thereby transient dips in the detected signal. A unique property of iFCS is its ability to determine the absolute volume of particles directly from the amount of displaced solution. Here, this ability was utilized with scanning-iFCS (siFCS) to determine the size of spots seven times smaller than the resolution of the microscope on surfaces. Equations were derived for obtaining the spot-size from the auto- and cross-correlation functions, measurements were simulated which enabled testing of these equations, and finally measurements were performed on model surfaces mimicking membranes with green labeled lipids and red labeled domains/protein clusters. By using a confocal microscope of 270 nm resolution the size of the 250 nm domains were estimated by siFCS/siFCCS to 257 ± 12 nm diameter, and the 40 nm domains were estimated to 65 ± 27 nm diameter. Comparison with previous iFCS-analyses indicates that confocal siFCS should be able to determine the size of spots down to 20 nm diameter, while STED-iFCS should determine spots well below 10 nm diameter.

INTRODUCTION

The plasma membrane is the site of a large number of molecular interactions crucial for the survival of the cell. Cell surface receptors span and transmit signals across the membrane and are often drug targets, such as in the case of the G-protein coupled receptor which is the target of about 40 % of all pharmaceutical drugs. As part of their normal function receptors cluster into oligomers. Such receptor clusters can sometimes be as large as 100 nm in diameter, but exist likely in all sizes down to dimers smaller than 5 nm diameter. Receptor clustering may occur inside so called lipid rafts which consist of glycosphingolipids and transmembrane proteins. Lipid rafts are

commonly believed to be 10-200 nm in diameter even though larger and smaller values also have been suggested.

Receptor clustering and lipid rafts are difficult to study because their sizes are below the diffraction limit of visible light. Confocal laser scanning microscopes (LSMs) have a resolution of about 250 nm and can therefore only determine the size of the largest clusters and domains. Analysis of those of smaller size has to rely on fluorescence intensity which is uncertain due to the strong fluorescence quenching often occurring in such clusters.

The super resolution techniques (STED, PALM/STORM) which have emerged during the last ten years allow the generation of fluorescence images with a resolution down to about 30 nm. This opens up for analysis of cluster- and raft-sizes that are inaccessible to confocal imaging, and especially the localization techniques are suitable for detection of clusters. However, dimers, trimers and tetramers which likely are the most common clusters are still too small to be distinguished. Moreover, the localization techniques are limited to analysis of fixed cells, and STED-imaging of living cells can only be performed on very limited areas of the cell. STED-FCS has been employed for analyzing nanodomains in living cells by varying the diameter of the detection area, but does not yield absolute sizes of domains.

Inverse FCS (iFCS) can be performed on a normal FCS instrument by detecting a signal from the fluorophores surrounding the particles of interest. IFCS was originally demonstrated on particles not smaller than 100 nm diameter dissolved in a concentrated dye solution. Shortly thereafter iFCCS was introduced where a signal from fluorescent particles (eg red) was cross-correlated with the signal from the surrounding fluorophores (eg green). In iFCCS the absolute volume of particles is conveniently given by the negative amplitude of the cross-correlation curve. Furthermore, iFCCS allows the labeled particles to be analyzed specifically even in the presence of other, non-labeled particles.

A fundamental difference between standard FCS and iFCS is that standard FCS estimates the size of particles indirectly from the diffusion coefficient, while iFCS measures the absolute volume directly from the amount of displaced fluorophores. iFCS thus gives an absolute value of the particle size, and is in addition more sensitive since the amplitude of the iFCS curve is proportional to the square of the particle volume, while the diffusion time in standard FCS scales with the cubic root of the particle mass.

Performing iFCS on a cell membrane would be very interesting because of the amount of fundamental interactions that take place there. The possibility to

apply iFCS to determine the absolute size of receptor clusters before and after stimulation of the same living cell would be very valuable. Furthermore, the iFCS technique itself would benefit from a two dimensional surface compared to 3D solution, since a larger fraction of the signal is displaced in a 2D situation (Wennmalm & Widengren 2011). When iFCS has been applied to 3D diffusion in solution, particles 500 times smaller than the detection volume (i.e. constituting 0.2 %) have been detected, in a diffraction limited focus as well as in nano-wells. Assuming that the same sensitivity can be achieved on a surface, it should be possible to determine the size of 18 nm diameter objects by a normal confocal microscope of 250 nm resolution. If instead a STED microscope is used which has a resolution of about 40 nm, then the same 1:500 ratio indicates that the size of 3 nm diameter objects can be determined.

Here, Scanning Inverse FCS (siFCS) is introduced to analyze immobile surfaces. The iFCS and iFCCS analysis on surfaces mimicking membranes indicates that membrane objects with a diameter at least seven times smaller than the resolution of the microscope used.

MATERIALS AND METHODS

Sample preparation

Fluorescent carboxylated nanoparticles (NPs) with excitation/emission spectrum of 580/605 (“green NPs”) or 625/605 (“red NPs”) were purchased from Life Technologies. The green NPs had a diameter of 200 nm or 36 nm and the red NPs a diameter of 250 nm or 40 nm.
Coverslips (22×22 mm and 0.13-0.16 mm thick) and microscope slides (26×76 mm and 1-1.2 mm thick) were purchased from Menzel-Gläser. Mowiol mounting medium was prepared according to a standard protocol.
A single layer of NPs was formed by first coating the coverslip with Poly-L-lysine (PLL, Sigma Aldrich) which resulted in a positively charged surface, followed by incubation of the negatively charged carboxylated NPs.
For the 250 nm NPs, the PLL-coating was generated by first cleaning the cover slip with a solution of 70 % ethanol and 1 % HCl, then draining in ultra pure water and drying with nitrogen. 100 μl of PLL diluted 1:10 in ultra pure water was incubated for 5 minutes and then washed in ultra pure water. The cover slips were left to dry at room temperature over night. The stock solutions of the 250 nm beads were diluted as follows: For the incubation of NPs onto the PLL-coated coverslips, green and red NPs were mixed in PBS buffer pH 7.3 such that 80 % of the NPs were green and 20% were red. 100 μl of this NP mixture was let to incubate on the PLL-coated cover slips for 20 minutes, followed by

washing richly but gently with carbonate buffer pH 8.3 to remove any additional layers of beads. The cover slips were then air dried at room temperature for about 2 hours. Finally the cover slips were mounted onto a microscope slide using 15 μl of Mowiol mounting medium.

For coupling of the 40 nm NPs, the cover slips were sonicated for 15 minutes in 2-propanol, then washed in ultra pure water and blow dried with nitrogen, then 100 μl of PLL was incubated for 5 minutes followed by washing in ultra pure water and air drying at room temperature over night. The NPs were mixed in PBS pH 7.3 such that 90 % of the NPS were green and 10% were red. Because the 40 nm beads were more likely to aggregate the NP mixture was sonicated for 20 minutes before incubation on the PLL-coated coverslips for 30 minutes. Thereafter the cover slips were washed with a pipette with carbonate buffer of pH 8.4, followed by air drying at room temperature for 2 hours. Finally the cover slips were mounted onto a microscope slide using 15 μl Mowiol mounting medium.

Microscope

The microscope used for confocal as well as STED images was a homebuilt two-colour laser scanning STED (Stimulated Emission Depletion) microscope which has been described in detail previously. For confocal imaging the resolution of the microscope was 270-290 nm FWHM, while for STED imaging the resolution was about 40 nm FWHM.

Simulations

A custom written MATLAB code was used for the simulations. Two images were generated by randomly distributing a given number of dots in each image, one corresponding to the red image and one corresponding to the green image. To simulate beads with a physical size each dot was given a radius, for example six pixels, which limited how close neighboring beads could be positioned. In this way no beads overlapped physically in the green or in the red image. This corresponded to a single layer of beads on the cover slip. Each dot was then given a normalized Gaussian intensity profile where the full width half maximum (FWHM) of the profile corresponded to the resolution of the microscope in the red and the green channel respectively. A number of parameters could thereby be adjusted freely: image size, bead sizes, number of red and green beads, and the resolution in the red and the green channel. In reality cross-talk is present when performing two-colour imaging. To simulate cross talk a fraction of the intensity in the green image was added to the red image and vice versa. By denoting the intensity in the green image I_{green} and the

intensity in the red image I_{red}, the intensity in the red image including cross-talk, called I_{red+CT} is given by

$$I_{red+CT} = I_{red} + fI_{green} \quad (1)$$

where f is the fraction of the signal in the green channel that is detected also in the red channel. For cross-talk in the green image the equation is the same but with the red and green subscripts switched. For our microscope the cross-talk is about 1% and the simulations including cross-talk were carried out using f = 0.005 or f = 0.01.

Noise was included by adding the absolute value of normally distributed random numbers to each pixel in each image. The noise was then tuned by scaling the standard deviation σ of the normal distribution. In this study σ = 0.2 which means that the background signal is slightly less than 20% of the intensity of a single bead since this intensity is scaled to 1. Based on a visual comparison of the simulated and the real images, this is likely a somewhat higher noise level than in the real case. This way of implementing noise does not include the Poisson distributed photon noise which is proportional to the square root of the intensity value at each pixel [6]. However if the noise can be assumed to be uncorrelated it should not enter into the correlation functions except in the dominator in Eq. 2.1 and Eq. 2.2 in Ch. 2. Only considering uncorrelated background noise might therefore be at least a quantitative indication of how noise influences the sizing.

Data analysis

Data analysis was carried out using MATLAB. Cross-correlation and auto-correlation curves were most quickly generated by a two dimensional fast Fourier transform (Eq. 2.5 in Ch. 2). The two dimensional correlation functions were projected onto the x- and y-plane and averaged over the projections. In this way the correlation functions were plotted as one dimensional curves which facilitates reading of the amplitudes $G_{CC}(0)$ and $G_{AC,r}(0)$, and furthermore it is computational faster to perform a one dimensional Gaussian fit.

The number of red beads in each image had to be counted in order to estimate the bead density. For this a MATLAB code was written which detects intensities in the image above a given cut-off value and then checks weather it is a bead or not. This MATLAB program counted the number of beads with an accuracy of about 95 %, and a few images were always counted manually as a double check.

In order to reduce cross-talk the microscope uses time-gated excitation and detection meaning that the green and red excitation lasers pulses are separated in time by 40 ns. The initial green excitation pulse excites the green fluorophores but also some of the red fluorophores. A fraction of the light from the red fluorophores will be detected by the green detector (this constitutes the cross-talk in the green channel), but most of it will be recorded by the red detector. In this way an image of the crosstalk in the green channel is created by the red detector. 40 ns later a red excitation pulse will excite mostly the red fluorophores but also some of the green fluorophores. A fraction of the light from the green fluorophores will be detected by the red detector (this constitutes the cross-talk in the red channel), but most of it will be recorded by the green detector. In this way an image of the crosstalk in the red channel is created by the green detector.
To compensate for cross-talk in the data analysis a fraction F of the cross-talk image I_{CT} was subtracted from the original image I_{orig} (see Fig. 3.1). This fraction was estimated by taking the average intensity I_r of a dark area in the original image divided by the average intensity I_{CT} of the same area in the corresponding cross-talk image. Thereby $F = I_r/I_{CT}$ and the cross-talk reduced image becomes

$$I_{reduced} = I_{orig} - F \cdot I_{CT} \qquad (2)$$

The value of Q turned out to be approximately 0.3 for both confocal and STED images. Note that this does not mean that the cross-talk is 30%, but that the cross-talk image records about 3 times more of the cross-talk than the actual image.

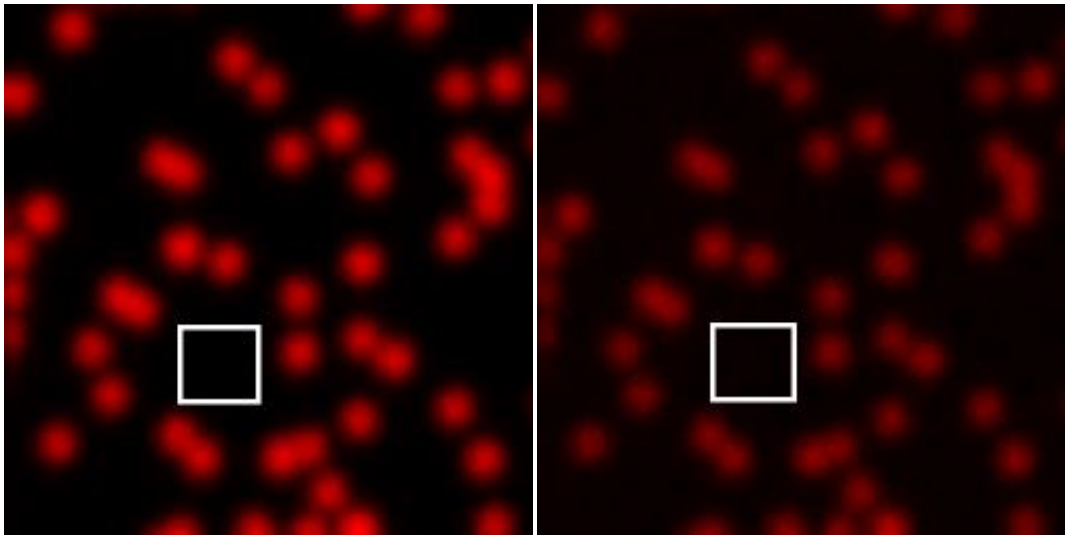

Figure 1. A typical image of red beads and the corresponding cross-talk image. The white square marks an area where the average intensity is compared

between the images. For this particular area the mean intensity in the original image (a) was $I_r \approx 5$ counts and the mean intensity in the cross-talk image (b) was $I_{CT} \approx 15$ counts giving $F \approx 0.3$, where F is the factor which the cross-talk image is multiplied with before subtracting it from the original image.

THEORY

Applying the theory of iFCCS for imaging requires that the ergodic principle holds in the sense that scanning over an immobilized surface is equivalent to particles fluctuating through a detection volume. Furthermore the particles should be uniformly randomly distributed on the surface so that the number of particles within the detection area is Poisson distributed (Petersen,…, Wiseman, …, K-E Magnuson, 1993).
With these two assumptions the theory of iFCCS was directly applied to scanned surfaces. When performing iFCCS on diffusing molecules it is the time dependent cross-correlation function that is analyzed, where the amplitude of the cross-correlation function reveals information about the volume of the diffusing particles. However when iFCCS is performed on a surface it is rather the two dimensional spatial cross-correlation function $G_{CC}(x, y)$ that will be considered, defined as

$$G_{CC}(x,y) = \frac{\langle \delta i_r(x'+x, y'+y)\delta i_g(x', y') \rangle}{\langle i_r(x', y') \rangle \langle i_g(x', y') \rangle} \quad (3)$$

where $i_r(x',y')$, $i_g(x',y')$ is the red and the green intensity respectively at a point (x',y') on the surface and $\delta i(x',y') = i(x',y') - \langle i \rangle$ is the fluctuation of the intensity around its mean value and $\langle \ldots \rangle$ is the spatial average taken by integrating over all the points (x',y').

The autocorrelation function for the red image $G_{AC,r}(x, y)$ will also be considered. It is defined in the same way as $G_{CC}(x, y)$ but with $g = r$ and thus becomes

$$G_{AC,r}(x,y) = \frac{\langle \delta i_r(x'+x, y'+y)\delta i_r(x', y') \rangle}{\langle i_r(x', y') \rangle \langle i_r(x', y') \rangle} \quad (4)$$

When referring to properties that are shared by the cross-correlation function and the auto-correlation function they will just be called the correlation functions $G(x, y)$. If the intensity of the detection area is assumed to have a

Gaussian intensity profile, then $G_{CC}(x, y)$ and $G_{AC,r}(x, y)$ should be fitted with a Gaussian function [5, 6, 7] given by

$$G_{fit}(x,y) = G(0)e^{-\frac{x^2+y^2}{\sigma}} + G_{\infty} \quad (5)$$

where $G(0)$, ∞ and G_{∞} are the fitting parameters. The offset G_{∞} has to be included since when obtaining the correlation function the data is restricted by the scanned area and the sampling intervals so enough data might not be sampled for the correlation functions to go to zero [5]. The parameter σ is the e^{-2}-decay which defines the radius of the detection area [5].

When an image is recorded by the microscope it will be represented by a matrix $i(k, l)$, $k, l = 1, 2, ..N$ where N is the total number of samplings intervals along the x and y-dimension, i.e. it is assumed to be a square image. Each element in this matrix will represent a pixel where the value of a pixel at point (k, l) is the intensity at that point. For this discrete set of intensities the spatial average is given by summing over all pixels and then dividing by the number of pixels so the discrete correlation function at point (k,l) becomes

$$G(k,l) = \frac{\frac{1}{(N-m)(N-n)}\sum_{m=1}^{N-k}\sum_{n=1}^{N-l}\delta i_s(m+k,n+l)\delta i_t(n,m)}{\frac{1}{N^2}\sum_{n=1,m=1}^{N} i_s(m,n)\frac{1}{N^2}\sum_{n=1,m=1}^{N} i_t(m,n)} \quad (6)$$

where $s = r$, $t = g$ for the cross-correlation function and $s = t = r$ for the autocorrelation function. This way of calculating the correlation functions numerically can be implemented directly in e.g. MATLAB. However, obtaining the correlation functions by a Fourier transform makes the computations considerably faster. The correlation function is then given by

$$G(k,l) = \frac{N^2 F^{-1}\left[F[i_s(m,n)]\cdot F^*[i_t(m,n)]\right]}{\sum_{n=1,m=1}^{N} i_s(m,n)\sum_{n=1,m=1}^{N} i_t(m,n)} \quad (7)$$

where F^{-1} is the inverse Fourier transform and * denotes the complex conjugate. The amplitude $G_{CC}(0)$ is the parameter that will be of the greatest interest for iFCCS since it gives the projected area of the particles on the surface [1], however also the amplitude $G_{AC,r}$ is needed. To see how $G_{CC}(0)$

depends on the particle area, consider a red particle that is fully within the green detection area A_g. It occupies an area A_p and reduces thereby the green intensity by a factor A_p/A_g where A_g is the area of the green detection focus, and the expression for the mean value of the green intensity becomes

$$\left\langle i_g \right\rangle = I_g = I_{g,tot}\left(1-\frac{A_p}{A_g}N_{pg}\right)+I_{g,CT} \tag{8}$$

and the mean value of the red intensity becomes

$$\left\langle i_r \right\rangle = I_r = Q_p N_{pr} + I_{r,CT} \tag{9}$$

where $I_{g,tot}$ is the total green intensity that would be detected if there were no red particles on the surface, N_{pr} and N_{pg} are the average number of red particles in the red respectively green detection area and Q_p is the intensity of each red particle. The last terms in each equation, $I_{g,CT}$ and $I_{r,CT}$ are the cross-talk terms that come from that a fraction of the red signal leaks over into the green channel and the other vice versa.
By assuming zero cross-talk and using that $\langle \delta i_r \delta i_g \rangle = \Delta I_r \Delta I_g$ where ΔI is the standard deviation of the Poisson distributed intensity fluctuations from particles within the detection area so that $\Delta N_{ps} = \sqrt{N_{ps}}$ ($s = r, g$), it follows that

$$\left\langle \delta i_r \delta i_g \right\rangle = \Delta\left(I_{g,tot}\left(1-\frac{A_p}{A_g}N_{pg}\right)\right)\cdot\Delta\left(Q_p N_{pr}\right) = -I_{g,tot}\frac{A_p}{A_g}Q_p\sqrt{N_{pg}N_{pr}} \tag{10}$$

Together with Eq. 2.6 and Eq. 2.7 and inserting it into the definition of $G_{CC}(x, y)$ (Eq. 2.1) for $(x, y) = 0$ gives the theoretical expression for the amplitude of the cross-correlation function for the ideal case of zero cross-talk

$$G_{CC}(0) = \frac{-I_{g,tot}\dfrac{A_p}{A_g}Q_p\sqrt{N_{pg}N_{pr}}}{Q_p N_{pr}\left(I_{g,tot}\left(1-\dfrac{A_p}{A_g}N_{pg}\right)\right)} = \frac{-A_p}{\sqrt{A_g A_r}\left(1-\dfrac{A_p}{A_g}N_{pg}\right)} \tag{11}$$

where in the last step the identity $N_{pr}/N_{pg} = A_r/A_g$ was used. The fact that the amplitude is negative indicates anti-correlation between the green and red channel.

If the particle size is much smaller than the detection area A_g and the particle density n is low so that $N_{pg} = nA_g < 1$ then $(A_p/A_g)N_{pg} = nA_p << 1$ and the amplitude can be approximated by

$$G_{CC}(0) \approx \frac{-A_p}{\sqrt{A_g A_r}} \tag{12}$$

which is a useful equation for estimating the particle size when the particle density is not known except for that it is low in the sense that $N_{pg} << 1$. These are the basic equations used to determine the particle size.
The detection area may be difficult to define exactly, since it may be defined by the e^{-2}-width or the e^{-1}-width or even by some other definition. Regarding the density of particles, it may in principle be determined by simply calculating the number of particles in the image, which is possible given that the separation of the particles is on average greater than the resolution of the microscope [3]. In this study the particles will always be countable and the red detection area A_r can therefore be estimated from the amplitude of the autocorrelation function for only the red image. For the red image the average number of particles N_{pr} in the red detection area is given by [5]

$$N_{pr} = \frac{1}{G_{AC,r}(0)} \tag{13}$$

where $G_{AC,r}(0)$ is the amplitude of the auto-correlation function for the red image. At the same time N_{pr} is given by

$$N_{pr} = \frac{A_r N_p}{A} = A_r n \tag{14}$$

where A is the area of the surface scanned by the microscope, N_p is the total number of particles in the red image and n is the total density of particles in the red image. Together equations 13 and 14 together give

$$A_r = \frac{1}{nG_{ac,r}(0)} \tag{15}$$

Therefore by determining $G_{AC,r}(0)$ and counting the number of particles in the red image the red detection area A_r can be estimated, without knowledge of the particle size. When A_r is estimated the green detection area A_g can also be estimated by assuming that the intensities in the foci of the red and green

lasers are distributed in the same way and that A_g is defined by the same cut-off as A_r for some decay width, e.g. full width at half maximum (FWHM) or the e^{-2} width. If some of these decay widths are known for both channels, here called ω_r respectively ω_g, then

$$A_g = \left(\frac{\omega_g}{\omega_r}\right)^2 \cdot A_r = \left(\frac{\omega_g}{\omega_r}\right)^2 \frac{1}{nG_{ac,r}(0)} \tag{16}$$

By inserting the expressions for A_r and A_g into Eq. 11 and solving for A_p the final equation for determining the particle area becomes

$$A_p = \frac{1}{n}\frac{\omega_g}{\omega_r}\left[-\frac{G_{ac,r}(0)}{G_{CC}(0)} + \frac{\omega_g}{\omega_r}\right]^{-1} \tag{17}$$

(note that the area will be positive since $G_{CC}(0) < 0$). To use this equation the widths of the foci must be known for both the red and green laser. For this study two types of imaging are used, confocal and STED, where the width is given by the FWHM of the foci (i.e. the resolution). For the confocal imaging it is ω_r = 280 nm and ω_g = 260 nm and for STED $\omega_r = \omega_g$ = 40 nm. Inserting these values into Eq. 17 and using that the particles are circular such that the diameter is given by $d = \sqrt{4A_p/\pi}$, gives the expression for size of spots on the surface in confocal images

$$d = \frac{2}{\sqrt{\pi}}\sqrt{\frac{1}{n}\frac{13}{14}\left[-\frac{G_{ac,r}(0)}{G_{CC}(0)} + \frac{13}{14}\right]^{-\frac{1}{2}}} \tag{18}$$

and in STED images

$$d = \frac{2}{\sqrt{\pi}}\sqrt{\frac{1}{n}\left[-\frac{G_{ac,r}(0)}{G_{CC}(0)} + 1\right]^{-\frac{1}{2}}} \tag{19}$$

These equations will be used for determining the size of spots on the surface, which in our case are the fluorescent beads. For this the amplitudes of the cross-correlation function and the auto-correlation function and the density of beads need to be known, which all can be obtained experimentally. Note that these equations were derived assuming that the cross-talk is zero, therefore it

will be important to reduce the cross-talk as much as possible in the experiments for these equations to be valid.

RESULTS

Simulations:
The simulated images were 5×5 μm and consisted of either 100×100 pixels corresponding to a step length of 50 nm as for confocal images, or they consisted of 250×250 pixels corresponding to a step length of 50 nm as for the STED images. The resolution of the confocal microscope of about 270 nm was simulated using a Gaussian intensity profile with FWHM of 6 pixels, while the STED resolution of 40 nm was simulated using a Gaussian intensity profile with a FWHM of 2 pixels. Comparing the simulated images with real images shows however that a width of 4 pixels was more realistic for the STED simulation (fig. 2).

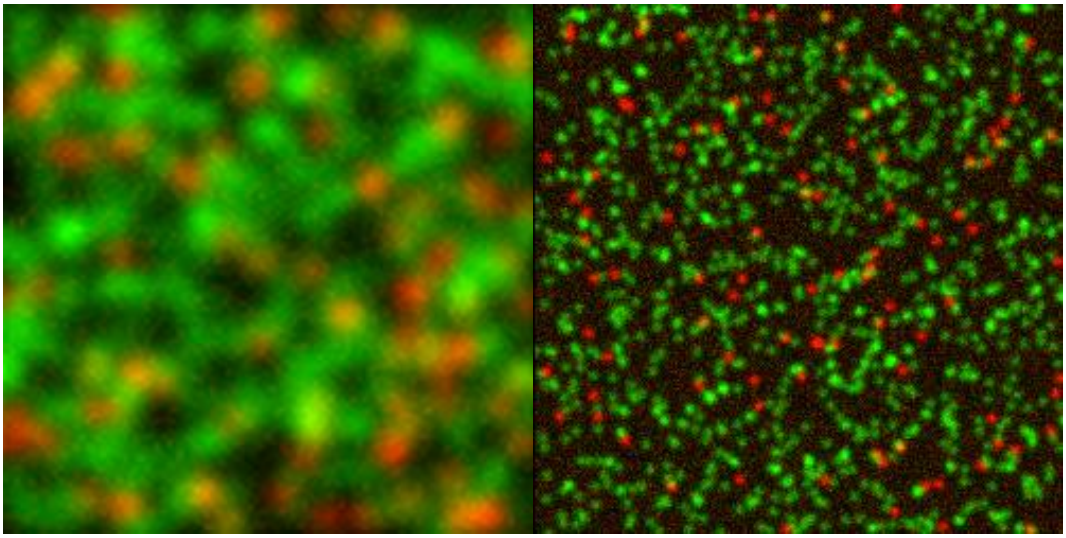

Figure 2. Simulated images, including noise, with 100 and 1000 red and green beads respectively. (a) Simulated confocal image. Image size was 100 × 100 pixels, bead size was 1 pixel and the resolution was 6 pixels. This corresponds roughly to confocal imaging of 40 nm beads (compare with fig. 9a). (b) Simulated STED image. The location of the beads is not the same as in (a). Image size was 250×250 pixels, bead size was 1 pixel and the resolution was 4 pixels. This corresponds roughly to STED imaging of the 40 nm beads (compare with fig. 9b).

Table 1 displays simulations where the number of red beads was kept constant at 50 and the number of green beads was varied, and three different bead sizes were simulated. The simulations indicate that as long as > 10 % of the surface is covered by green beads, the bead size estimated from $G_{CC}(0)$ has a standard deviation not exceeding ~30%, even when realistic levels of noise and cross-

talk were included. However, the bead size is over estimated at low total concentrations which is likely an effect of the increased gap between beads.

Table 1. Simulations of confocal images with varying densities of green beads.

Percentage of total area covered by beads (# green beads)	Bead size	Estimated size without noise and cross-talk	Estimated size with noise and cross-talk added
5% (590)	1	1.7 ± 0.7 (54)	1.7 ± 0.7 (12)
10% (90)	3	3.4 ± 1.1 (84)	3.0 ± 1.0 (66)
20% (50)	5	5.4 ± 0.8 (99)	4.5 ± 1.0 (97)
40% (150)	5	5.4 ± 0.5 (100)	5.3 ± 0.5 (100)
80% (360)	5	4.9 ± 0.3 (100)	5.5 ± 0.3 (100)

The resolution was 6 pixels corresponding to a confocal microscope, for images of size 100×100 pixels with a total of 50 red beads in each image. 100 images were generated for each simulation. The cross-talk was 1%. The error is the standard deviation. The value in parenthesis after the size estimate is the total number of images yielding a cross-correlation curve with negative amplitude used for the size estimation.

For small bead sizes, another effect at low total concentrations was that the cross-correlation curves sometimes had positive amplitude, even when no noise or cross-talk was added to the images. A likely explanation for this effect is that in those cases the intensity profiles of the red and the green beads overlap to the extent that the net result is a positive correlation. This issue will be further investigated below. If only curves with negative amplitude were taken into account when calculating the average $G_{CC}(x)$ the obtained sizes from using Eq. 17 were reasonable and within the standard deviation, however, if all curves were used then the amplitude was reduced (fig 3).

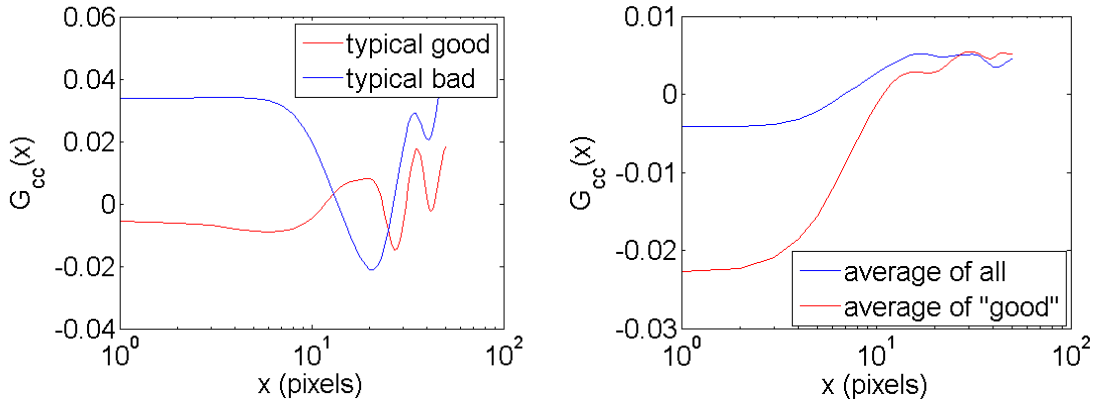

Figure 3. Cross-correlation curves for simulated images containing 100×100 pixels. The bead size is 1 pixel and the number of red and green beads is 100 and 1000 respectively. The resolution was 6 pixels. (a) Examples of single-image cross-correlation curves. A curve with

positive amplitude (blue) and a curve with negative amplitude (red) are shown. (b) Average correlation curves for 100 images: of all cross-correlation curves (blue) and of all cross-correlation curves with negative amplitude, 53 in total.

For the simulated confocal images, the phenomenon of cross-correlation curves with positive amplitude was most frequently observed when the bead size was 1 pixel (46 out of 100 images, table 1), corresponding to a bead size of 50 nm. In order to investigate this phenomenon further, a second series of images were simulated at different concentrations of green beads, where the beas size was always 50 nm, confocal and also STED images, with our without cross-talk and noise. For the images without cross-talk and noise, a lower concentration of green beads resulted in a higher chance of a positive cross-correlation amplitude (table 2). This is possibly because the increased variance of the cross-correlation curves at lower concentrations results in a larger fraction of curves with positive amplitude. Again, lower concentrations of green beads resulted in over estimation of the (red) bead size. Summarizing the estimations without cross-talk and noise, sizing of the 50 nm beads was satisfactory when the concentrations of green beads was above 1000 beads per 5x5 μm area.

Cross-talk and noise were added to the images (table 2); 1% cross-talk for the confocal simulations and 0.5% for the STED simulations (a value of 1% cross-talk in the STED simulations was also tested but resulted in no anti-correlation at all). The addition of cross-talk increased the number of positive cross-correlation amplitudes, as expected since cross-talk appearing in the red image correlates positively with the original green image, and vice versa for cross-talk from the red to the green image. This resulted in fewer images yielding anti-correlation and a reduced average cross-correlation amplitude. As a result of this cross-talk effect, lower concentrations of green beads resulted in fewer cross-correlation curves with positive amplitude, i.e. the opposite of the situation with no cross-talk (table 2). Thus, when cross-talk and noise are added the beads are over estimated at low concentrations of green beads and under estimated at high concentrations of green beads. This emphasizes the importance of minimizing cross-talk during imaging and compensating for cross-talk in the analysis.

Table 2. Simulation with 100 red beads in each image. The bead size is 1 pixel. Each simulation generated 100 images and the error is the standard deviation. The value in parenthesis following the estimated size is the number of images yielding cross-correlation curves with negative amplitude used for the size estimation. (a) Confocal and STED simulations. Confocal simulations was done with image size 100 × 100 pixels and resolution 6 pixels. STED simulations was done with image

size 250 × 250 pixels and resolution 4 pixels. (b) Same as in (a) but with noise and cross-talk added. The cross-talk is 1% for the confocal simulations and 0.5% for the STED simulations (higher values gave very few images yielding anti-correlation). For 9000 green beads no STED images gave anti-correlation. The noise is tuned so it is about 20% of the intensity per bead.

(a) Simulations without noise or cross-talk

# Green beads	Bead size	Estimated size Confocal	Estimated size STED
100	1	2.2 ± 0.9 (51)	2.0 ± 0.8 (61)
300	1	1.7 ± 0.7 (53)	1.7 ± 0.7 (77)
1000	1	1.3 ± 0.5 (52)	1.3 ± 0.5 (76)
3000	1	1.0 ± 0.4 (55)	1.2 ± 0.4 (84)
9000	1	1.0 ± 0.3 (60)	1.1 ± 0.2 (96)

(b) Simulations with noise and cross-talk added

# Green beads	Bead size	Estimated size Confocal	Estimated size STED
100	1	2.1 ± 0.8 (44)	2.6 ± 1.1 (36)
300	1	1.6 ± 0.8 (42)	2.1 ± 0.7 (28)
1000	1	1.2 ± 0.4 (34)	1.8 ± 1.0 (19)
3000	1	0.9 ± 0.5 (19)	1.4 ± 0.6 (10)
9000	1	0.6 ± 0.4 (8)	

As mentioned earlier the likely explanation for the positive cross-correlation amplitudes in images without cross-talk or noise is the overlap between the intensity profiles of the red and the green beads (fig. 4). This is supported by the fact that the number of cross-correlation curves yielding anti-correlation is higher for the STED simulations, where the intensity profile is narrower, than for the confocal simulations (table 2a).

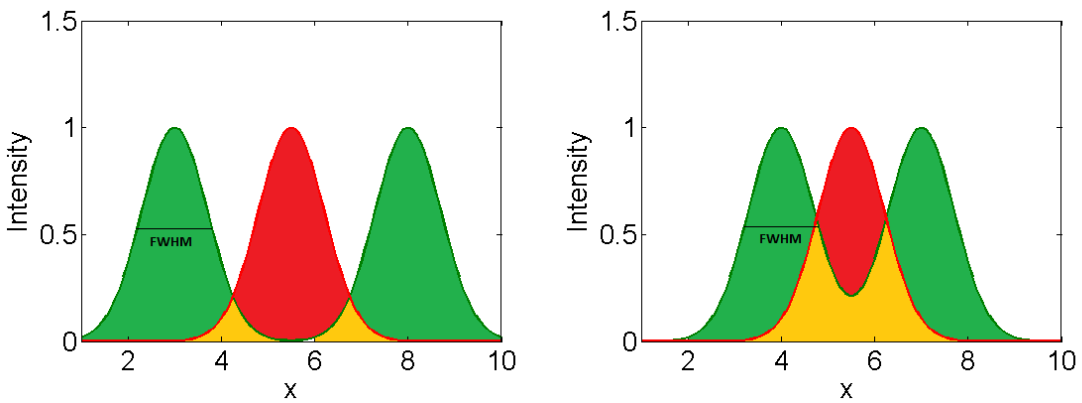

Figure 4. The intensity profiles of two green beads surrounding one red bead.

The yellow areas indicates the overlap of the intensity profiles were there might be a positive contribution to the cross-correlation amplitude. (a) Small overlap of the intensity profiles. (b) Large overlap of the intensity profiles.

To further confirm this hypothesis a third series of simulations of 50 nm beads were performed, without cross-talk and noise, with a resolution varying from a FWHM of 2 to 12 pixels, with 100 simulations for each resolution (table 3). As expected, when the FWHM of the beads increased the number of positive cross-correlation amplitudes increased.

Table 3. Simulation without noise and cross-talk for different resolution and with image size 100 × 100 pixels and bead size 1 pixel. Number of red beads is 100 and number of green beads is 1000. The number of generated images was 100 for each simulation and the error is the standard deviation.

Width (FWHM)	# Images yielding anti-correlation	Bead size	Estimated size
2	99	1	1.1 ± 0.3
4	69	1	1.1 ± 0.4
6	52	1	1.3 ± 0.5
8	46	1	1.4 ± 0.6
10	24	1	1.3 ± 0.5
12	16	1	1.4 ± 0.7

EXPERIMENTS

250 nm beads

A total number of 14 confocal and STED images were recorded for the 250 nm Beads (fig 5). An intensity trace of the confocal image shows how the red peaks coincide with the green dips (fig 5, right). The resolution of the STED-microscope, about 40 nm in lateral direction, was sufficient to resolve individual 250 nm beads (fig. 5). Multiple layers of beads were rarely seen and could easily be identified in STED-images (fig 5, middle, arrow).

The theoretical expression for the amplitude of the cross-correlation curve (eq. 2.9) assumes that the presence of a red bead in the detection area reduces the green signal in proportion to the projected area of the bead. However, when the red 250 nm beads are imaged with the STED-microscope they are larger than the detection area and the theory does not hold. Therefore only the confocal images are considered for the 250 nm beads.

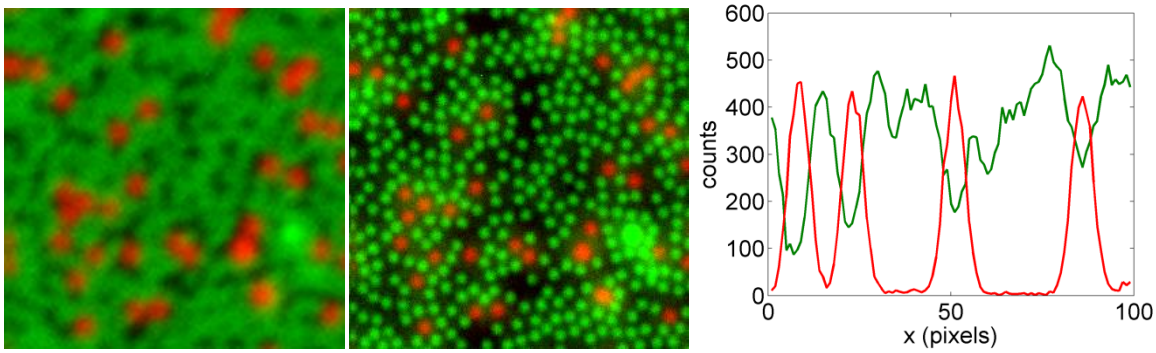

Figure 5. Typical confocal and STED image of the same scanned area on the cover slip. The size of the scanned area is 5 × 5 μm. The white arrow in (b) points out an area on the surface were the beads most likely has formed a multiple layer. However in this images this multiple layer is very small compared to the total area and has very little effect on the analysis. (c) Trace for arbitrary line in the confocal image.

The red and green images were cross-correlated to obtain $G_{CC}(0)$ and the red image was auto-correlated to obtain $G_{AC,r}(0)$ (fig 6). By counting the red beads in each image the density of red beads was estimated to be $n = 1.97 \pm 0.32 \times 10^{-6}$ beads/nm^2, where the error is the standard deviation. This gave all the parameters needed in eq. 17 to estimate the diameter d of the red beads. The beads covered about 60% of the surface and therefore comparison with the simulations (table 1) indicates that all images should yield anti-correlation. This was also observed.

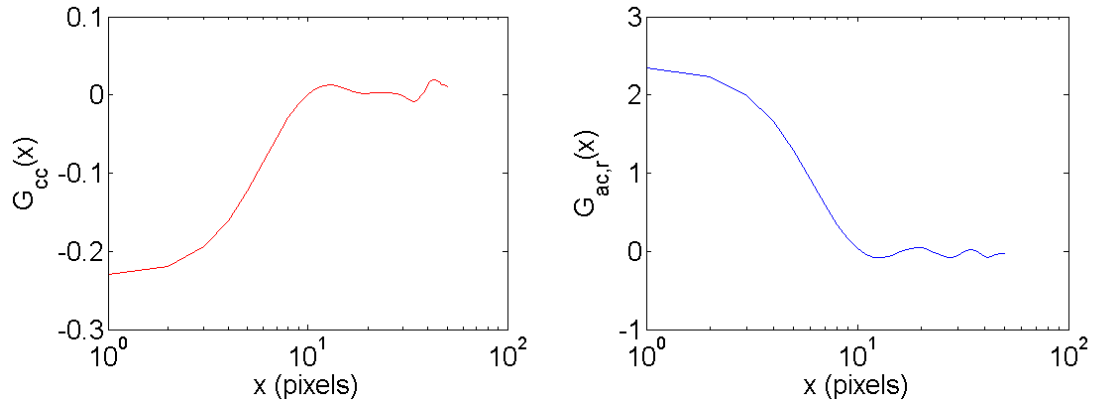

Figure 6. Typical cross correlation curve (a) and auto-correlation curve (b) for a single image of the 200 nm beads. The unit on the x-axis is pixels where 1 pixel = 50 nm.

According to the theory the curves should be fit with a Gaussian (Ch. 2). This is done for the average cross-correlation curve and average auto-correlation curve (average means that all the curves for each image has been summed together and divided by the number of images) and are shown in Fig. 4.6.

The cross- and auto-correlation curves from all images were averaged and thereafter fitted with the Gaussian fitting function (eq. 5). The Gaussian fit of both averaged curves yielded amplitudes of $G_{CC}(0) = -0.22$ and $G_{AC,r}(0) = 1.95$ (fig 7). Both fits also yielded the same e^{-2} – decay widths of 267 nm. Using this as the radius of the detection area [6] resulted, according to eq. 13, in the density 2.3×10^{-6} beads/nm^2 which differs by only 15 % to the density 1.97×10^{-6} beads/nm^2 obtained by counting. Thus the cross-talk present has only a minor effect on the size estimation. Inserting these values for the amplitudes and the mean density of 1.96×10^{-6} beads/nm^2 into eq. 18 gave an average diameter of the red beads of d = 246 nm which is close to the specified value 250 nm.

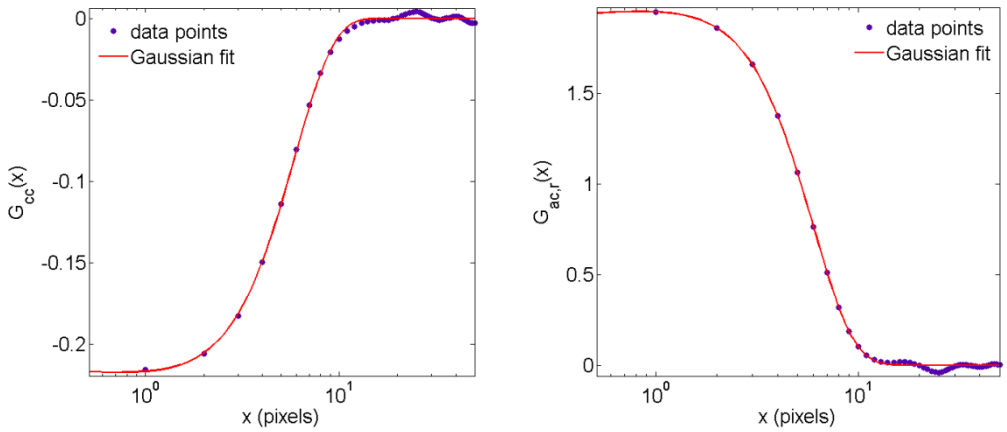

Figure 7. Average cross correlation curve and auto correlation curve for all 14 raw images of the 250 nm beads. The Gaussian fit of the data points gives the amplitudes as $G_{CC}(0) = -0.22$ and $G_{AC,r}(0) = 1.95$ which is the same as the raw data gives. The decay width at e^{-2} is the same for both curves and is 267 nm. The unit on x-axis is in pixels were 1 pixel = 50 nm.

If the size was instead estimated from each individual image followed by averaging over all estimates, then d = 248 ± 17 nm where the error is the standard deviation.

Next we investigated the effect of compensating for cross-talk as described in the data analysis section above. Following this procedure and estimating the diameter of the beads from each image after reducing for cross-talk and averaging gave

d = 257 ± 12 nm

This result is slightly overestimated but the specified value is still within the standard deviation, which is now slightly smaller (5%). Averaging instead all correlation curves for the cross-talk reduced images (Fig. 4.7) gives $G_{CC}(0) = -0.27$ and $G_{AC,r}(0) = 2.15$ which gives the size d = 259 nm using $n = 1.97\times10^{-6}$

beads/nm^2. The e^{-2}-decay width is 270 nm for both of the curves which is about the same as for the raw images. Estimating the radius of the detection area from the e^{-2}-decay width together with $G_{AC,r}(0) = 2.15$ and eq. 13 gave the density as 2.0×10^{-6} beads/nm^2 for the red beads, which is very close to the density obtained by counting (a difference of 1.5%).

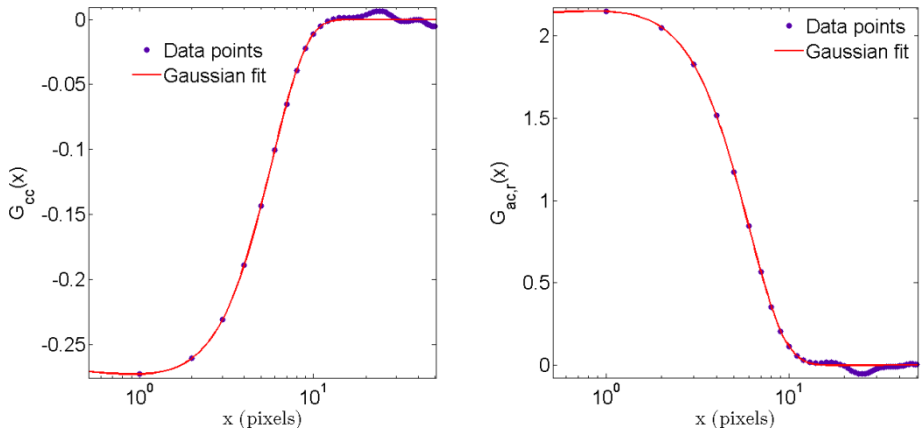

Figure 8. Average cross correlation curve and auto correlation curve for all 14 cross-talk reduced images of the 250 nm beads. The Gaussian fit of the data points gave the amplitudes as $G_{CC}(0) = -0.27$ and $G_{AC,r}(0) = 2.15$ which is the same as the raw data gives. The decay width at e^{-2} was 270 nm for both curves. The unit on x-axis is in pixels were 1 pixel = 50 nm.

Multiplying together the density with the area of the red beads gave $n \cdot A_p = 1.97 \times 10^6 \cdot \pi \cdot 125^2 = 0.01$, indicating that 1 % of the area was covered by red beads. Since $n \cdot A_p << 1$ it can be interesting to test the approximation given by eq. 12. Using the values of $G_{CC}(0)$ and the e^{-2}-decay width = 270 nm as the radius for the detection area gave an approximation of the diameter for raw and cross-talk reduced images respectively of

$$d = \frac{2}{\sqrt{\pi}} \sqrt{(13/14) \cdot \pi \cdot 270^2 \cdot 0.22} = 244 \text{ nm}$$

$$d = \frac{2}{\sqrt{\pi}} \sqrt{(13/14) \cdot \pi \cdot 270^2 \cdot 0.27} = 270 \text{ nm (cross-talk reduced)}$$

which are good estimations for the bead size. The slight overestimation of the cross-talk reduced images is again likely due to gap between the beads.

Finally, deconvolution by a built in function in MATLAB which uses the Richardson-Lucy algorithm was tested. Applying this onto the images and performing the size estimation gave $d = 250 \pm 17$ nm.

40 nm beads

The 40 nm beads have a diameter which is the same or slightly smaller than resolution of the STED microscope, and siFCS analysis can therefore be performed using either confocal microscopy or STED microscopy. The 40 nm sample has about 1000 green beads and 100 red beads in a scanned area of 5×5 μm, indicating that only about 10% of the area was covered by beads (fig 9). However, the earlier described simulations for these sizes and densities indicate that size estimation should still be possible though a slight overestimation may occur due to the low concentration. Intensity traces taken along the diagonal in the confocal and STED image are shown (fig. 10).

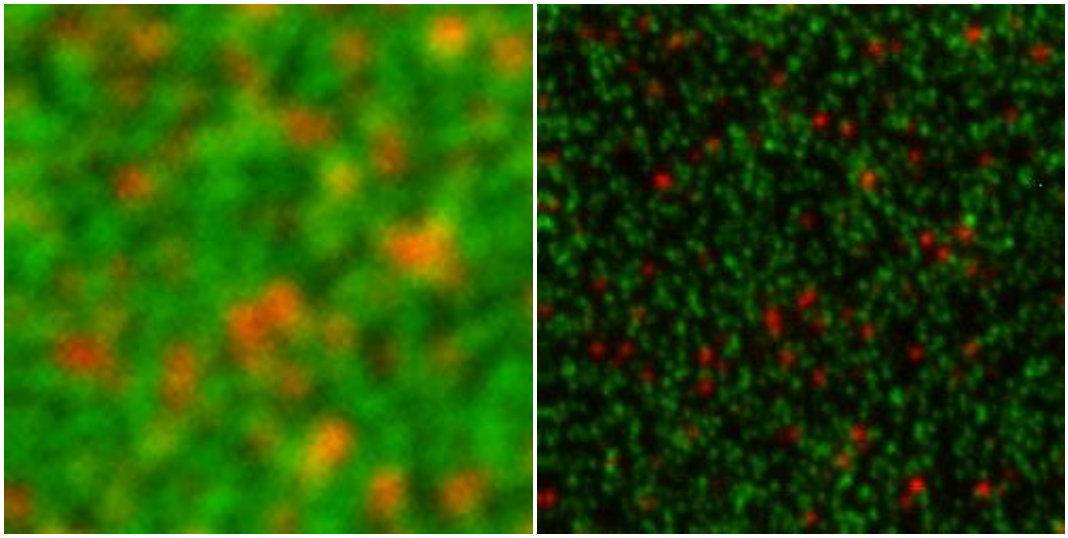

Figure 9. Typical confocal and STED images of the same 5 × 5 μm area of 40 nm beads. In the confocal image the individual beads cannot be resolved because of the resolution of ~270 nm (compare with fig. 5a). For the STED image the ~40 nm resolution can almost distinguish individual beads.

A total of 42 images were recorded. When the raw data of these images was analyzed in the same way as the 250 nm beads, 19 of the cross-correlation curves had negative amplitude, for the confocal as well as for the STED images. Negative cross-correlation amplitudes were not necessarily obtained from the same confocal and STED images. Following the result from the simulations above and only considering those images that gave a negative amplitude of the cross-correlation curve, and estimating the size for each individual image and then averaging gave for the confocal images d = 63 ± 25 nm and for the STED images d = 43 ± 8 nm.

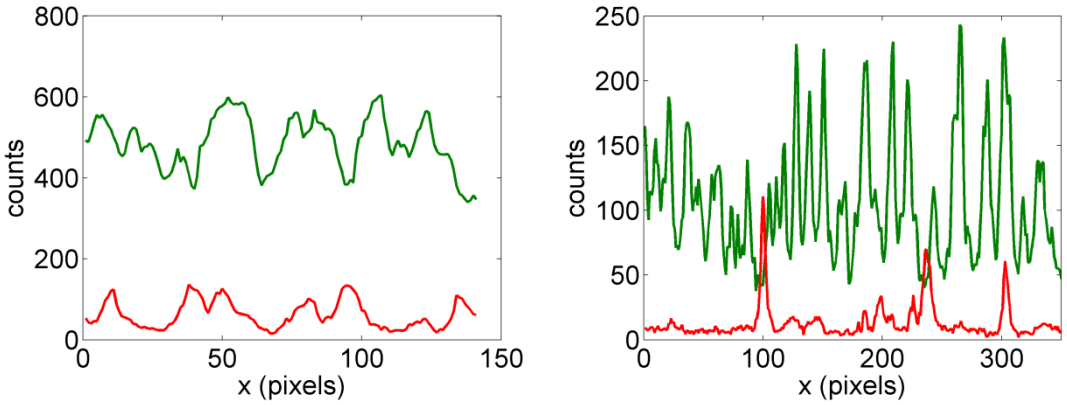

Figure 10. (a) The intensity trace for a line drawn on the diagonal in a confocal image of 40 nm beads. (b) The same intensity trace as in (a) for the STED image of the same area.

The STED images gave a better result and a smaller standard deviation which could be a result of the higher resolution of the STED microscope. Still, for the confocal images the specified size was within the standard deviation.

Averaging all the anti-correlation amplitudes and the corresponding auto-correlation amplitudes gave the mean amplitudes for confocal images $G_{CC}(0) = -0.0079$ and $G_{AC,r}(0) = 0.4631$. The e^{-2} -decay width for the cross-correlation curve was 410 nm and that for the autocorrelation curve 290 nm. Counting the red beads in each image gave a density $n = 4.16 \pm 0.37 \times 10^{-6}$ nm^{-2}, where the error is the standard deviation. Using these values together with eq. 17 gave the estimated bead size as $d = 69$ nm for raw confocal images.

For STED imaging a Gaussian fit of the average correlation curve (fig. 11c,d) gave the amplitudes $G_{CC}(0) = -0.013$ and $G_{AC,r}(0) = 1.98$ and the e^{-2}-decay width for the cross-correlation curve was 156 nm and for the autocorrelation curve 170 nm. Using these values together with the density 4.16×10^{-6} nm^{-2} gave the estimated bead size $d = 45$ nm for raw STED images.

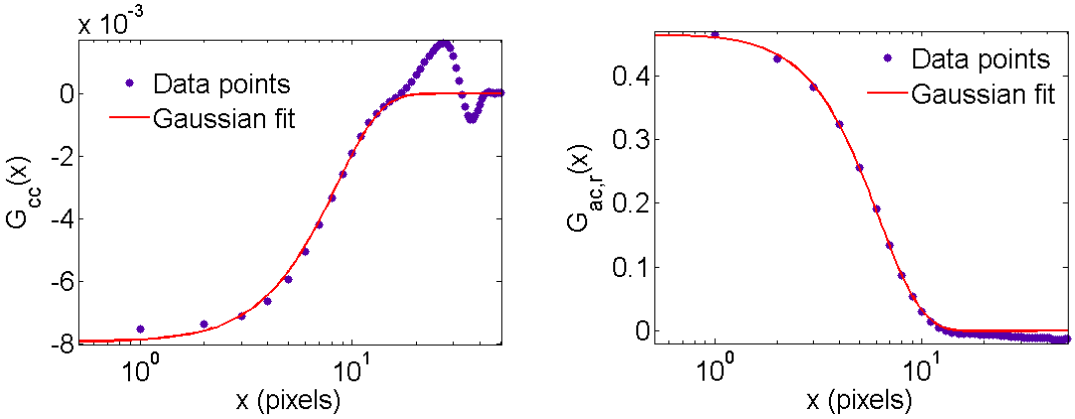

(a) Cross-correlation (confocal, raw) (b) Auto-correlation (confocal, raw)

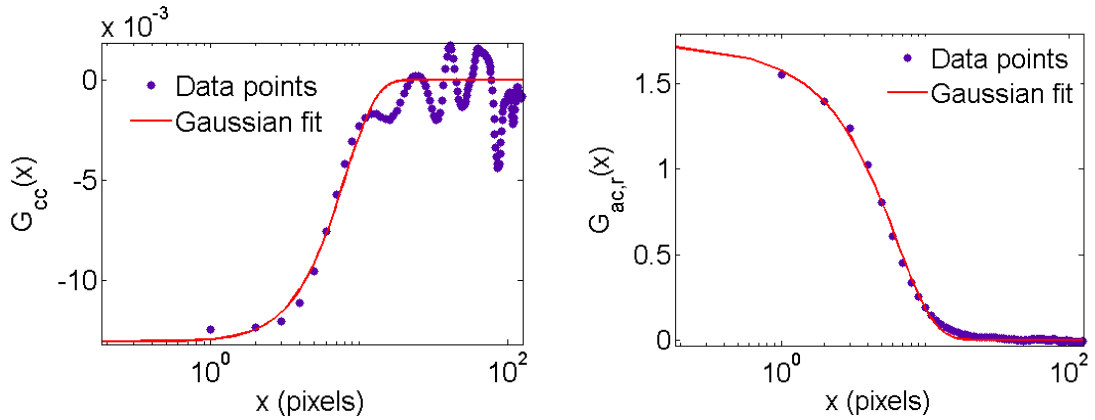

(c) Cross-correlation (STED, raw) (d) Auto-correlation (STED, raw)

Figure 11. (a) and (b): Average cross-correlation curve and auto-correlation curve for all raw confocal images yielding anti-correlation, 19 out of 42, of the 40 nm beads. The Gaussian fit of the data points gives the amplitudes as $G_{CC}(0) = -0.08$ and $G_{AC,r}(0) = 0.46$. The decay width at e^{-2} is for the cross-correlation curve 410 nm and for the auto-correlation curve 290 nm. The two differ about 30%. The unit on x-axis is in pixels were 1 pixel = 50 nm. (c) and (d): Same as in (a) and (b) but STED images yielding anti-correlation, 19 out of 42. The Gaussian fit of the data points gives the amplitudes as $G_{CC}(0) = -0.013$ and $G_{AC,r}(0) = 1.98$. The decay width at e^{-2} is for the cross-correlation curve 156 nm and for the auto-correlation curve 170 nm which differ about 9%. The unit on x-axis is in pixels were 1 pixel = 20 nm.

Compensation for cross-talk was attempted for the 40 nm beads as well using the same approach as for the 250 nm beads. This resulted in anti-correlation for 29 of the confocal images and 38 of the STED images. Estimating the size of the red beads from each individual image and then averaging gave for the confocal images

$d = 65 \pm 26$ nm

and for the STED images

$d = 76 \pm 17$ nm

For the STED images the size estimation deviates more from the specified 40 nm than the estimate from the raw data, however the Gaussian fit of the average curves (fig. 13) is somewhat better when cross-talk is compensated for. Furthermore the overestimation of the bead size is expected since the beads are not packed densely enough. The amplitudes of the average confocal cross-

talk reduced curves were $G_{CC}(0) = -0.013$ and $G_{AC,r}(0) = 0.73$ and the e^{-2}-decay widths were 335 nm for the cross-correlation curve (fig. 13 a) and 290 nm for the auto-correlation curve (fig. 13 b). Using these values gave the value d = 69 nm from the cross-talk-compensated confocal images. For the STED images the corresponding amplitudes were $G_{CC}(0) = -0.12$ and $G_{AC,r}(0) = 1.98$ and the decay widths at e^{-2} were 156 nm and 154 nm for the cross- and auto-correlation curves respectively (fig 13 c,d), which yielded an estimated diameter of 75 nm.

The cross-correlation functions for cross-talk compensated confocal images of the 250 nm and 40 nm beads are shown in the same graph for comparison (fig 12). As can be seen the amplitude for the 40 nm curve is about 20 times smaller than the 250 nm curve as expected from theory.

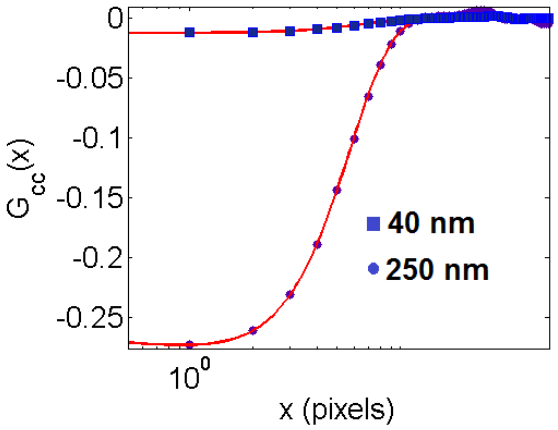

Figure 12. Cross-correlation curves from the confocal images of the 250 nm and 40 nm beads with Gaussian fits. The amplitude for the 250 nm curve is -0.27 and for the 40 nm curve the amplitude is -0.013. The unit on the x-axis is in pixels where 1 pixel = 50 nm.

In an attempt to further improve the cross-talk reduced images they were deconvolved with the Richardson-Lucy algorithm. In the subsequent cross-correlation analysis 26 of the confocal images and 40 of the STED images yielded anti-correlation out of the total 42 images. Thus the statistics should be somewhat better for the deconvoluted images than for the raw data. This was also expected since the positive cross-correlation amplitudes are a result of overlap between the red and green intensity profiles, and the width of the intensity profiles are reduced by deconvolution.

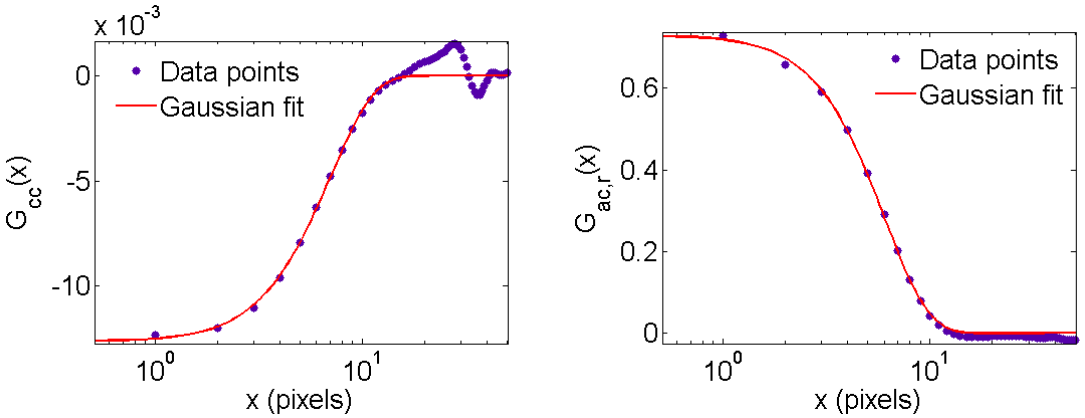

a) CC, confocal, cross-talk reduced b) AC, confocal, cross-talk reduced

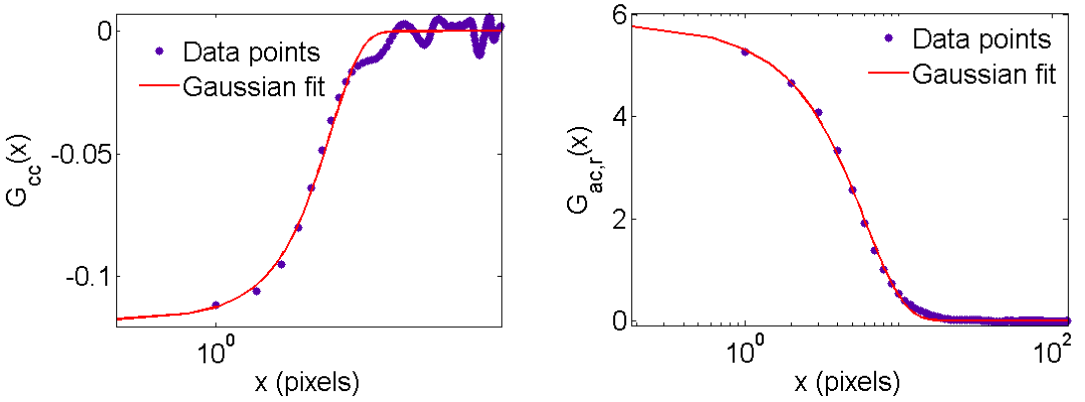

b) CC, STED, cross-talk reduced d) AC, STED, cross-talk reduced

Figure 13. (a) and (b): Average cross- and auto-correlation curves for all cross-talk reduced confocal images of the 40 nm beads yielding anti-correlation, 29 out of 42. The amplitudes were $G_{CC}(0) = -0.013$ and $G_{AC,r}(0) = 0.73$. The decay widths at e^{-2} were 335 nm and 290 nm for the cross- and the auto-correlation curves respectively. The unit on x-axis is in pixels where 1 pixel corresponds to 50 nm. (c) and (d): Same as in (a) and (b) but STED images yielding anti-correlation, 38 out of 42. The amplitudes were $G_{CC}(0) = -0.12$ and $G_{AC,r}(0) = 6.46$. The decay widths at e^{-2} were 156 nm and 154 nm for the cross- and the auto-correlation curves respectively. The unit on x-axis is in pixels where 1 pixel corresponds to 20 nm.

The result of the size estimation was

$d = 51 \pm 19$ nm (Confocal, cross-talk compensated and deconvoluted)

$d = 59 \pm 17$ nm (STED, cross-talk compensated and deconvoluted)

The estimates are closer to the specified values which are within the standard deviation but the relative standard deviations are about the same (~50%).

Averaging over all the anti-correlation curves and over the corresponding auto-correlation curves resulted for the confocal images in $G_{CC}(0) = -0.029$ and $G_{AC,r}(0) = 1.78$ which yielded a diameter of 68 nm. The e^{-2}-decay widths for the confocal curves were 173 nm and 200 nm for the cross- and auto-correlation curves respectively (fig 14 a,b). The average cross-correlation curve from the confocal images had a dip at about x = 100 nm. Similar dips were sometimes observed also for individual images in the simulations, but disappeared after averaging over several images (fig 3). This effect could therefore be a result of limited statistics.

For the STED images the amplitudes were $G_{CC}(0) = -0.38$ and $G_{AC,r}(0) = 26.8$ which yielded a diameter of 65 nm. This auto-correlation amplitude was about five times higher than that of the non-deconvoluted auto-correlation curve. This could be a result if beads that are less bright disappeared due to the deconvolution, leaving a strongly reduced apparent concentration. Furthermore the detection area was reduced since the effective resolution was enhanced, as can be seen from the e^{-2}-decay widths of 69 nm and 65 nm respectively (fig 14 c, d).

Since $n \cdot A_p = 4.16 \times 10^{-6}\ \text{nm}^{-2} \cdot \pi \cdot 20^2\ \text{nm}^2 = 0.005 << 1$, the approximation in eq. 12 was tested for size-estimation. Using $G_{CC}(0) = -0.013$ for confocal and $G_{CC}(0) = -0.12$ for STED from the cross-talk reduced images and using the e^{-2}-decay widths ~290 nm and ~150 nm for the confocal and STED detection areas respectively [6] yielded

$$d \approx \frac{2}{\sqrt{\pi}}\sqrt{\pi \cdot 290^2 \cdot 0.013}\ \text{nm} = 66\ \text{nm} \qquad \text{(confocal)} \quad (4.12)$$

$$d \approx \frac{2}{\sqrt{\pi}}\sqrt{\pi \cdot 150^2 \cdot 0.12}\ \text{nm} = 104\ \text{nm} \qquad \text{(STED)} \quad (4.13)$$

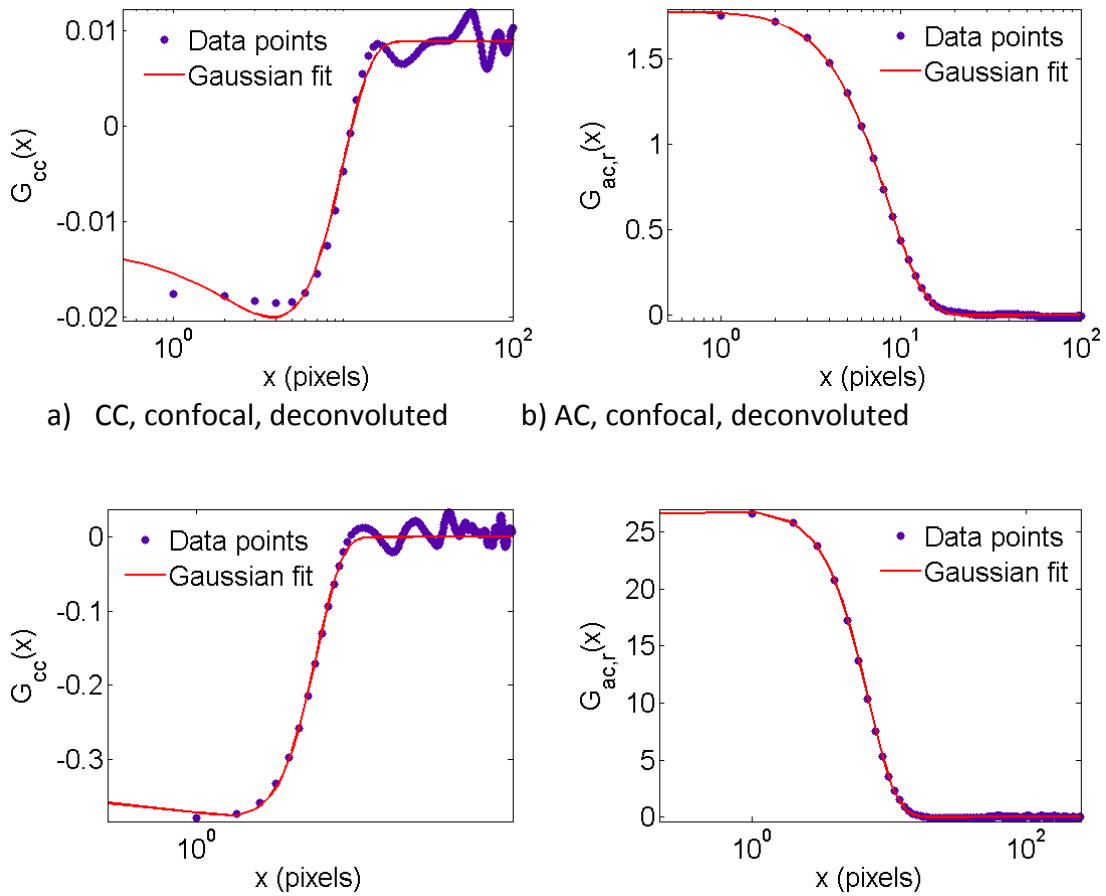

Figure 14. (a) and (b): Average of all anti-correlation curves (26 out of 42) for the deconvoluted and cross-talk compensated confocal images of the 40 nm beads. The amplitudes were $G_{CC}(0) = -0.029$ and $G_{AC,r}(0) = 1.78$. The decay widths at e^{-2} were 173 nm and 200 nm for the cross- and auto-correlation curves respectively. The unit on x-axis is in pixels where 1 pixel = 25 nm. (c) and (d): Same as in (a) and (b) but STED images yielding anti-correlation (40 out of 42). The amplitudes were $G_{CC}(0) = -0.38$ and $G_{AC,r}(0) = 26.8$. The decay widths at e^{-2} were 69 nm and 65 nm for the cross- and auto-correlation curves respectivley. The unit on x-axis is in pixels were 1 pixel = 10 nm.

DISCUSSION

Even though the gaps between the 40 nm beads could not be avoided siFCS analysis was possible using a confocal microscope with a resolution of 270 nm FWHM. If the gaps had been smaller or even absent the sizing would have been more accurate and the error would have been smaller. Therefore the results indicate that if gap-free samples can be prepared, for example by fluorescence labeling of the phospholipids in bilayers or cells, then it should be possible to determine the size of domains smaller than 40 nm.

This is also the indication when a comparison is done with previous iFCS analyses. In the first demonstration of iFCS nanoparticles down to 100 nm

diameter could be analyzed in a 0.3 fL detection focus, indicating that particles could be detected as long as the particle to detection volume-ratio did not exceed about 1 to 500 (Wennmalm et al 2009). The same 1 to 500 ratio was observed when iFCS was used to analyze protein molecules with a volume of 250 nm^3, which were the smallest particles that could be analyzed in nanowells with a volume of $1.2 \cdot 10^{-4}$. If the same ratio can be reached on a surface it should be possible to determine the size of domains with a diameter of about 20 nm using confocal imaging, and below 5 nm diameter using STED imaging.

iFCS was applied by scanning real or simulated fixed surfaces mimicking membranes consisting of green labeled phospholipids and red labeled domains/clusters. Super-resolution imaging of fixed cells is routinely performed using STED- and PALM/STORM-imaging. Standard STED microscopes have a resolution of about 40 nm while state of the art microscopes can image cells with a resolution of about 30 nm. The PALM/STORM localization techniques can come down to a resolution of about 20 nm. Since transmembrane proteins have a diameter of 2-3 nm, there is thus still a need for techniques that can determine the size of clusters and domains in the range 1-20 nm.

More importantly, iFCS on surfaces should be equally applicable to living cell membranes or fluid lipid bilayers. Sizing of domains, or clusters of proteins, in dynamic membranes or live cells has a significant advantage compared to sizing in fixed cells. Not only is perturbation of the living cell avoided, it allows the on-line addition/removal of substances and monitoring their effect on the size of the nanodomains.

In summary, we have demonstrated that iFCS can be applied to fixed surfaces to determined the absolute size of domains on the surface. Using a confocal microscope with a resolution of 270 nm FWHM, the projected area of fluorescent beads with a specified diameter of 250 nm was estimated to 257 $\pm$ 12 nm and the projected area of beads with a specified diameter of 40 nm were estimated to 65 $\pm$ 26 nm. The deviation of the latter estimate from the specified value relates to the mean distance between beads on the surface. For the 40 nm beads STED imaging could also be used for sizing, but was more sensitive to the presence of gaps between beads.
iFCS has the potential to become very useful for determining sizes of domains, rafts and protein clusters below 10 nm diameter in fluid or fixed membranes.

REFERENCES

[1] S. Wennmalm, J. Widengren, *Inverse-Fluorescence Cross-Correlation Spectroscopy*, Anal. Chem. **82** 5646-5651 July (2010).
[2] O. Krichevsky, G. Bonnet, *Fluorescence correlation spectroscopy: the technique and its applications*, Rep. Prog. Phys. **65** 251-29, January (2002).
[3] S. W. Hell, *Far-Field Optical Nanoscopy*, SCIENCE **316** 1153-1158 May (2007).
[4] S. Wennmalm, P. Thyberg, L. Xu, J. Widengren, *Inverse-Fluorescence Correlation Spectroscopy*, Anal. Chem. **81** 9209-9215 November (2009).
[5] N. O. Petersen, P. L. Höddelius, P. W. Wiseman, O. Seger, K-E. Magnusson, *Quantitation of Membrane Receptor Distributions by Image Correlation Spectroscopy: Concept and Application*, Biophys. J. **65** 1135-1146, September (1993).
[6] S. Costantino, J. W.D Comeau, D. L. Kolin, O. Seger, P. W. Wiseman, *Accuracy and Dynamic Range of Spatial Image Correlation and Cross-Correlation Spectroscopy*, Biophys. J. **89** 1251-1260, August (2005).
[7] D. L. Kolin, P. W. Wiseman, *Advances in Image Correlation Spectroscopy: Measuring Number Densities, Aggregation States, and Dynamics of Fluorescently labeled Macromolecules in Cells*, Cell Biochem. Biophys. **49** 141-164, October (2007).
[8] Z. Földes-Papp, U. Demel, G. P. Tilz. *Laser scanning confocal fluorescence microscopy: an overview* International Immunopharmacology **3** 1715-1729 May (2003)
[9] https://science.nichd.nih.gov/confluence/display/mic/MOWIOL+Mounting+Media
[10] http://www.cncro.net/en/training/mowoil-mounting-medium
[11] http://research.abl.es/methods/1453/mowiol-aqueous-mounting-media/
[12] D. Wildanger, E. Rittweger, L. Kastrup, S. W. Hell, *STED microscopy with a supercontinuum laser source* Optics Express **16** 9614-9621 June (2008).
[13] D. Wildanger, J. Bückers, V. Westphal, S. W. Hell, L. Kastrup, *A STED microscope aligned by design* Optics Express **17** 16100-16110 August (2009).
[14] D. Wildanger, R. Medda, L. Kastrup, S. W. Hell, *A compact STED microscope providing 3D nanoscale resolution* Journal of Microscopy **236** 35-43 October (2009).